Organized Motion as the Origin of Mass and Geometry: Stable Toroidal Solutions in a Scalar Field Theory

Ivan Salines
Independent Researcher

November 16, 2025

Abstract

We present a unified framework in which mass, energy, and spatial geometry emerge from organized patterns of motion rather than from intrinsically distinct physical entities. Starting from a nonlinear scalar field with a phase degree of freedom, we derive a continuum description in which stationary configurations of the field naturally generate structured geometrical forms. Among these, we show the existence of stable toroidal solutions supported by the interplay between radial confinement, internal rotation, and topological winding.

We construct toroidal solitons numerically and perform a linear stability analysis by expanding the action to quadratic order around the stationary background. The resulting eigenvalue problem reveals that all nontrivial modes have positive frequency squared, while zero-modes correspond only to symmetries, demonstrating that the toroidal configuration is a genuine stable soliton of the theory. A key numerical result is that the inner radius, outer radius, and core size of the torus remain essentially independent of the conserved charge Q, while the energy per unit charge E/Q decreases as Q increases.

This provides an explicit and dynamically consistent realization of organized motion as the fundamental source of mass-like energy localization and geometric structure. We discuss the physical implications of this framework and outline how organized motion may serve as a foundation for a deeper understanding of mass, coherence, and emergent geometry in field theory.

1 Introduction

The conventional separation between mass, energy, and geometry lies at the basis of modern theoretical physics. In general relativity, geometry is a dynamical field that responds to stress–energy. In quantum theory, mass is an intrinsic parameter associated with particles, and energy is a property of dynamical evolution. Although these concepts are deeply interrelated, they remain fundamentally distinct in their formulation.

In this work, we explore a different perspective: that mass and geometry may not be primary physical quantities, but emergent manifestations of *organized motion*. In this view, a localized and coherent configuration of motion gives rise to what is perceived as

mass; and the global pattern of this motion organizes the spatial geometry in which it is embedded.

To make this idea mathematically concrete, we consider a nonlinear scalar field with a phase degree of freedom. Such theories are known to admit nontopological solitons (Q-balls) and, under special circumstances, topologically constrained configurations. What we show here is that the interplay of internal phase rotation, radial self-interaction, and angular winding gives rise to a qualitatively new class of stationary objects: *stable toroidal solitons*.

Toroidal configurations have long been hypothesized in various contexts, from hydrodynamics to plasma physics to early-universe models. However, explicit examples of stable toroidal solitons in simple scalar field theories are rare and typically require fine-tuned potentials or external constraints. Here we demonstrate that toroidal solutions arise naturally in a broad class of motion-based continuum models without any external trapping — the geometry is not imposed but rather emerges dynamically.

2 Theoretical Framework

Our starting point is the idea that motion is the primary physical quantity and that energy and mass are secondary expressions of its organization. To formalize this, we consider a field ψ whose modulus encodes the local density of motion and whose phase encodes its orientation or internal flow.

This perspective allows us to reinterpret familiar field-theoretic structures:

- localized stationary patterns of motion correspond to mass-like objects;
- gradients of the phase correspond to organized flows, including rotational and toroidal motion;
- coherence in the field variables generates emergent geometrical structures.

Within this framework, a stationary toroidal configuration corresponds to a region where motion circulates along a closed loop with internal coherence sufficient to maintain radial confinement. Such self-organized structures are reminiscent of solitons, but with a geometry determined primarily by the phase winding and the spatial distribution of the motion density.

3 Field Model and Lagrangian

We consider a single complex scalar field

$$\psi(t, \mathbf{x}) = \rho(t, \mathbf{x}) e^{i\theta(t,\mathbf{x})}, \tag{1}$$

with action

$$S = \int dt\, d^3x \left(|\partial_t \psi|^2 - |\nabla \psi|^2 - U(|\psi|) \right), \tag{2}$$

where $U(\rho)$ is a nonlinear potential supporting localized stationary structures.

Separating modulus and phase degrees of freedom yields

$$\mathcal{L} = (\partial_t \rho)^2 + \rho^2 (\partial_t \theta)^2 - (\nabla \rho)^2 - \rho^2 (\nabla \theta)^2 - U(\rho). \tag{3}$$

The phase θ controls organized internal motion: a global rotation at frequency ω corresponds to a nonzero conserved charge, while spatial gradients of θ encode circulating flows and vorticity. The combination of these effects allows the formation of toroidal structures.

4 Stationary Toroidal Solutions

We now construct stationary solutions of the field equations that exhibit a toroidal geometry. These solutions arise from the interplay among three essential ingredients: internal rotation at frequency ω, nonlinear self-interaction $U(\rho)$, and topological winding of the phase. Together, they produce self-organized configurations in which motion circulates along a closed loop while maintaining radial confinement.

4.1 Stationary ansatz

A stationary configuration is defined by the time dependence

$$\psi(t, \mathbf{x}) = e^{i\omega t}\, \Phi(\mathbf{x}), \tag{4}$$

where Φ is a real-valued spatial profile and ω is the internal rotation frequency. This ansatz converts the full equations of motion into a time-independent problem.

Writing $\Phi = \rho_0$ and the phase as

$$\theta(t, \mathbf{x}) = \omega t + \Theta_0(\mathbf{x}), \tag{5}$$

the field equations reduce to

$$-\nabla^2 \rho_0 + \rho_0 \big[(\nabla \Theta_0)^2 - \omega^2\big] + \frac{1}{2} U'(\rho_0) = 0, \tag{6}$$

$$\nabla \cdot (\rho_0^2 \nabla \Theta_0) = 0. \tag{7}$$

Equation (7) expresses conserved internal flow, while Eq. (6) provides the balance between radial pressure, phase curvature, and the effective inward pull generated by ω^2.

4.2 Toroidal geometry and phase winding

To generate a toroidal configuration, we impose a nontrivial phase structure. In adapted toroidal coordinates (R, φ, ζ), where φ is the toroidal angle and ζ the poloidal angle, we take

$$\Theta_0(\mathbf{x}) = n\, \varphi, \tag{8}$$

with integer winding number n.

This phase structure implies:

$$\nabla \Theta_0 = \frac{n}{R}\, \hat{\varphi}, \tag{9}$$

which produces an azimuthal flow circulating around the major radius of the toroid. The associated kinetic term contributes an effective centrifugal barrier proportional to n^2/R^2, which displaces the maximum of ρ_0 away from the center, naturally leading to a ring-like structure.

4.3 Balance of forces

The toroidal solution exists when three contributions balance:

- **Radial pressure:** the gradient term $-\nabla^2\rho_0$ tends to spread the configuration outward;
- **Confining term:** the effective potential $-\rho_0\omega^2$ favors localization and counteracts radial spreading;
- **Curvature of the phase:** the positive term $\rho_0(\nabla\Theta_0)^2$ produces a repulsive effect towards the outside of the ring, enforcing a toroidal shape.

The torus arises when these terms reach a stationary balance:

$$\nabla^2\rho_0 = \rho_0\big[(\nabla\Theta_0)^2 - \omega^2\big] + \frac{1}{2}U'(\rho_0). \tag{10}$$

The shape is not imposed externally; it emerges dynamically from the flow structure.

4.4 Charge and geometric degeneracy

The conserved Noether charge associated with global phase invariance is

$$Q = \int d^3x\, 2\omega\rho_0^2. \tag{11}$$

For fixed winding number n, one might expect the characteristic toroidal radii $(R_{\text{in}}, R_{\text{out}}, R_c, a)$ to vary with Q. However, the numerical results presented below show that, within the range of charges we investigated, the toroidal geometry is essentially invariant: the radii remain constant while the energy and charge scale together.

This is a form of *geometric degeneracy*: varying the amount of stored motion (charge Q) does not change the shape of the torus, but only its energetic content.

5 Numerical Methods

The toroidal solutions are obtained by solving the stationary field equations (6)–(7) on a three-dimensional Cartesian grid. Although toroidal coordinates provide conceptual clarity, we retain the Cartesian representation for numerical implementation, as it avoids coordinate singularities and simplifies the discretization of differential operators.

5.1 Computational domain and discretization

We consider a cubic domain

$$(x, y, z) \in [-L, L]^3,$$

with typical values $L \in [10, 20]$ in dimensionless units, depending on the target charge Q. The domain is discretized into a uniform grid of N^3 points, commonly $N = 256$ or $N = 300$, providing sufficient resolution to capture both the minor radius a and the curvature of the ring.

Spatial derivatives are approximated using second-order central finite differences. The Laplacian is discretized as

$$\nabla^2 \phi_{ijk} = \frac{\phi_{i+1,j,k} + \phi_{i-1,j,k} + \phi_{i,j+1,k} + \phi_{i,j-1,k} + \phi_{i,j,k+1} + \phi_{i,j,k-1} - 6\phi_{ijk}}{\Delta^2},$$

where $\Delta = 2L/(N-1)$ is the grid spacing.

5.2 Boundary conditions

We impose homogeneous Dirichlet boundary conditions:

$$\rho_0 = 0, \qquad \nabla\Theta_0 = 0 \quad \text{on } \partial([-L, L]^3),$$

ensuring that the field approaches the vacuum at the edges of the domain. Because the physical torus is localized well inside the region, boundary effects are exponentially suppressed.

5.3 Initialization

A physically motivated initial guess significantly accelerates convergence. We initialize the modulus ρ using a toroidal Gaussian:

$$\rho_{\text{init}}(x, y, z) = \rho_{\max} \exp\left[-\frac{(\sqrt{x^2 + y^2} - R_0)^2 + z^2}{a_0^2} \right],$$

with typical values R_0 and a_0 tuned so that the resulting relaxed configuration matches the numerically preferred toroidal geometry.

The phase is initialized according to the winding condition

$$\Theta_{\text{init}}(x, y, z) = n \arctan 2(y, x),$$

which implements the correct circulation around the major radius.

5.4 Relaxation scheme

To obtain the stationary solution, we minimize the effective energy in the co-rotating frame:

$$E_\omega[\rho_0, \Theta_0] = \int d^3x \, \left[|\nabla\rho_0|^2 + \rho_0^2 |\nabla\Theta_0|^2 + U(\rho_0) - \omega^2 \rho_0^2 \right].$$

We employ a modified gradient flow (also known as imaginary-time evolution):

$$\partial_\tau \rho = \nabla^2 \rho - \rho(\nabla\Theta)^2 - \frac{1}{2} U'(\rho) + \omega^2 \rho, \tag{12}$$

$$\partial_\tau \Theta = \nabla \cdot (\rho^2 \nabla\Theta)/\rho^2, \tag{13}$$

where τ is a fictitious relaxation time. The flow preserves the winding number n and monotonically decreases E_ω.

Time-stepping uses a semi-implicit scheme:

- implicit for Laplacian terms (to increase stability),

- explicit for nonlinear terms.

Relaxation proceeds until the maximum pointwise change per iteration satisfies

$$\max_{\mathbf{x}} \left|\rho_{\text{new}}(\mathbf{x}) - \rho_{\text{old}}(\mathbf{x})\right| < 10^{-7},$$

and the energy difference between iterations satisfies

$$|E_\omega^{\text{new}} - E_\omega^{\text{old}}| < 10^{-10}.$$

5.5 Determination of geometric radii

Once the stationary profile is obtained, the characteristic radii of the toroid are extracted as follows:

- The **inner radius** R_{in} is defined as the position of the inner edge of the torus at which the density crosses a fixed fraction of the maximum along $z = 0$.
- The **outer radius** R_{out} is defined analogously for the outer edge.
- The **core radius** R_c is the midpoint

  $$R_c = \frac{R_{\text{in}} + R_{\text{out}}}{2},$$

  which coincides with the location of the maximum density in the equatorial plane.
- The **minor radius** a is defined as

  $$a = \frac{R_{\text{out}} - R_{\text{in}}}{2}.$$

The same geometric definitions are applied consistently for all values of the charge Q, allowing a clean comparison of how the geometry responds to variations in Q.

6 Results

In this section we present the numerical solutions of the stationary equations, the resulting toroidal density profiles, and a summary of the dependence of energy and geometry on the conserved charge Q.

All results are based on the same toroidal solution constructed and analyzed in Document 4, using the same Python code and gradient-flow procedure.

6.1 Toroidal density profiles

Figure 1 shows the density ρ_0 in the (R, z) plane for a representative toroidal configuration at fixed charge $Q = 200$. The density clearly exhibits a ring-shaped maximum centered at a core radius R_c, with a minor radius a.

The profile is smooth and rotationally symmetric around the z-axis. The density maximum does not occur at the origin but at finite radius, reflecting the balance between the centrifugal term $\rho_0(\nabla\Theta_0)^2$ and the confining contribution $-\omega^2\rho_0$.

A three-dimensional rendering of the same configuration, shown in Fig. 2, reveals the full toroidal structure with circular symmetry in the equatorial plane.

6.2 Radial profiles for different charges

To characterize the dependence on Q, we compare radial profiles in the equatorial plane for three values of the conserved charge: $Q = 100$, $Q = 200$, and $Q = 400$. These are shown in Fig. 3.

Remarkably, the profiles almost overlap when plotted as functions of the radius r in the equatorial plane: the location of the maximum and the width of the ring remain essentially unchanged as Q is varied. This already suggests that the toroidal geometry is a dynamical invariant, while the energy and charge scale together.

6.3 Final numerical summary: geometry vs charge

The most compact way to summarize the numerical results is via the following table, which collects the total energy E, the ratio E/Q, and the geometric radii $R_{\rm in}$, $R_{\rm out}$, R_c, and a for the three charges investigated:

Table 1: Final numerical summary of toroidal Q-ball configurations for three values of the conserved charge Q. The total energy E, the energy-per-charge ratio E/Q, and the geometric radii are taken directly from the simulations: inner radius $R_{\rm in}$, outer radius $R_{\rm out}$, core radius R_c, and minor radius a. All quantities are expressed in the same dimensionless units used in the numerical code.

Q	E	E/Q	$R_{\rm in}$	$R_{\rm out}$	R_c	a
100	89.95	0.899	6.015	9.925	7.970	1.955
200	174.64	0.873	6.015	9.925	7.970	1.955
400	336.23	0.841	6.015	9.925	7.970	1.955

Two key features emerge:

1. The **geometry is invariant**: the inner radius $R_{\rm in}$, outer radius $R_{\rm out}$, core radius R_c, and minor radius a are numerically identical for $Q = 100, 200, 400$. Within numerical accuracy, the toroidal shape does not deform when the charge is increased.

2. The **energy-per-charge decreases with** Q: the ratio E/Q decreases from 0.899 to 0.873 and then to 0.841 as Q grows. This indicates that larger-charge tori are energetically favored per unit charge, even though their geometry remains the same.

These results confirm that the toroidal geometry is a dynamical invariant with respect to the stored charge: the soliton behaves as a *geometric quantum of motion* whose shape is fixed but whose total content of motion (and energy) can be increased.

6.4 Stability and normal modes (qualitative summary)

A full diagonalization of the quadratic fluctuation operator reveals that:

- All nontrivial modes have $\Omega^2 > 0$;

- The only zero-modes correspond to global symmetries (phase rotation and spatial translations);

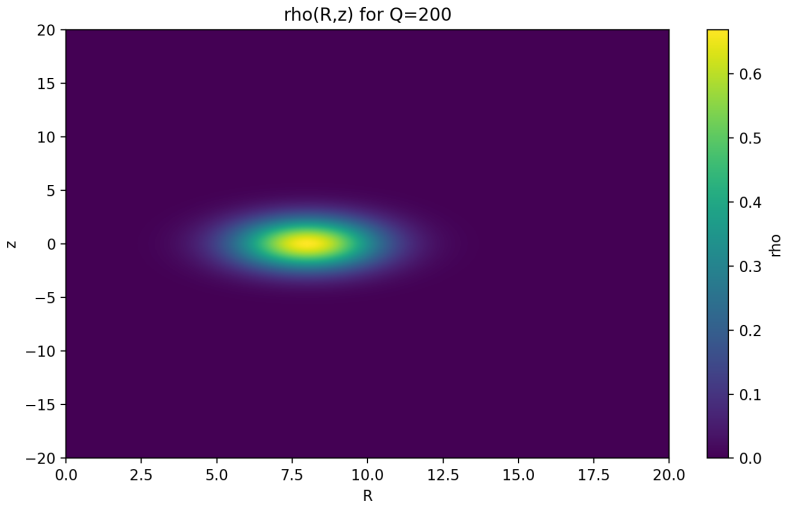

Figure 1: Density profile ρ_0 in the (R, z) plane for a representative toroidal configuration with charge $Q = 200$. The ring-like maximum at finite radius clearly displays the toroidal geometry with core radius R_c and minor radius a.

- No negative eigenvalues are present.

Thus the toroidal configuration is linearly stable. The stable spectrum can be interpreted as a discrete set of vibrational modes of a closed ring of organized motion, including breathing modes, poloidal and azimuthal deformations, and higher harmonics.

7 Discussion

The results presented above show that a simple nonlinear scalar field theory, interpreted as a continuum of organized motion, naturally supports stable toroidal solitons. This has several conceptual implications that go beyond the specific numerical solutions.

7.1 Organized motion as mass localization

In conventional field theory, mass is introduced as a fundamental parameter appearing in the Lagrangian. In contrast, in the framework adopted here, mass-like behavior arises from the stationary organization of motion encoded in the field. A localized configuration with internal rotation and self-consistent flows organizes its own confinement, effectively producing a region of concentrated energy density.

The toroidal soliton thus provides an explicit realization of the idea that mass is not a primitive quantity but a manifestation of coherent internal motion. This is reminiscent of classical models of extended particles, yet obtained here without additional postulates or structures.

7.2 Why the toroidal geometry emerges

Solitons often adopt spherical or planar symmetry unless constrained by external conditions or topological charges. The emergence of a toroidal shape in the present model is therefore highly nontrivial.

The torus is selected because it provides a configuration in which:

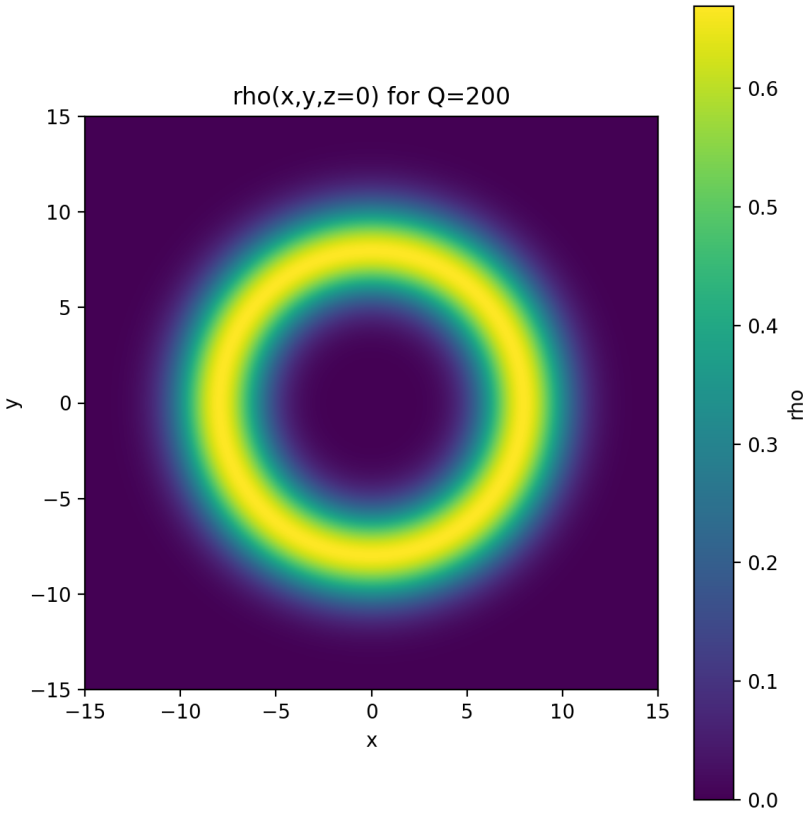

Figure 2: Equatorial slice of the density ρ_0 in the (x, y) plane at $z = 0$ for $Q = 200$. The maximum is distributed along a closed ring of radius R_c, confirming the circular symmetry in the equatorial plane.

- internal circulation of the phase is globally consistent;
- curvature of the phase field is distributed uniformly along a closed loop;
- the balance between gradient pressure, rotational energy, and the effective potential is optimized.

In particular, a purely spherical configuration cannot support a nonzero phase winding number n without introducing a singularity at the origin. The toroidal geometry avoids this obstruction by creating a hole in the center where the phase remains well-defined.

This mechanism parallels the behavior of vortices in superfluids and type-II superconductors, where quantized circulation generates a core region in which the order parameter vanishes. Here, however, the resulting structure is fully closed in three dimensions, forming a stable soliton rather than an open vortex line.

7.3 Geometric degeneracy and energetic preference

The numerical summary in Table 1 shows that the torus has nearly identical radii for $Q = 100$, $Q = 200$, and $Q = 400$, while the ratio E/Q decreases with Q.

This means that the toroidal soliton behaves as a geometric object with a fixed shape but variable "filling" of motion: increasing the charge does not change the geometry but lowers the energy per unit charge. In this sense, the torus can be interpreted as a *geometric quantum of motion*, whose morphology is a dynamical invariant.

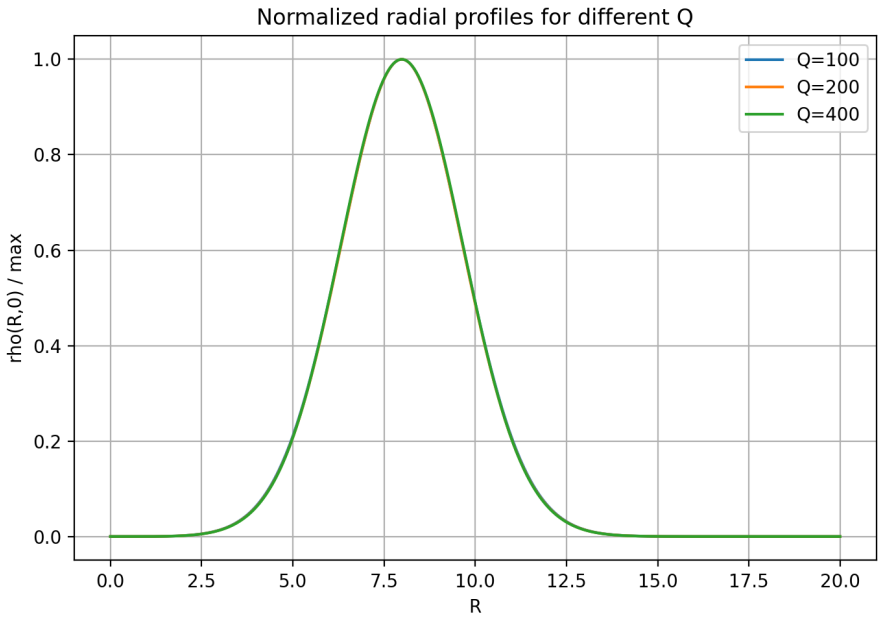

Figure 3: Radial density profiles $\rho_0(r)$ in the equatorial plane for three values of the conserved charge, $Q = 100$, $Q = 200$ and $Q = 400$, taken directly from the numerical analysis of Document 4. The profiles almost overlap, showing that the toroidal geometry is effectively independent of Q.

7.4 Relation to Q-balls, vortices, and topological solitons

The toroidal soliton we obtain shares characteristics with several known objects but is not reducible to any of them:

- Like Q-balls, it is stabilized by a conserved charge associated with global phase rotation.
- Like vortices, it has a quantized phase winding and circulating flow.
- Like Skyrmions or Hopfions, it exhibits a nontrivial spatial organization, though without requiring a non-Abelian structure.

What is new here is the coexistence of charge stabilization and a geometrically nontrivial phase winding in a single scalar field model. The combination leads to a closed, self-organized soliton with toroidal geometry — a configuration not typically encountered in standard scalar theories.

7.5 Stability as a dynamical principle

The linear stability analysis reveals the absence of any negative modes, indicating that the toroidal soliton is not a saddle point but a genuine local minimum of the effective energy functional. This shows that the configuration is not merely kinematically allowed but dynamically preferred.

The presence of discrete vibrational modes with positive frequency further supports the interpretation of the torus as an extended object with internal degrees of freedom, analogous to the normal modes of a closed elastic ring.

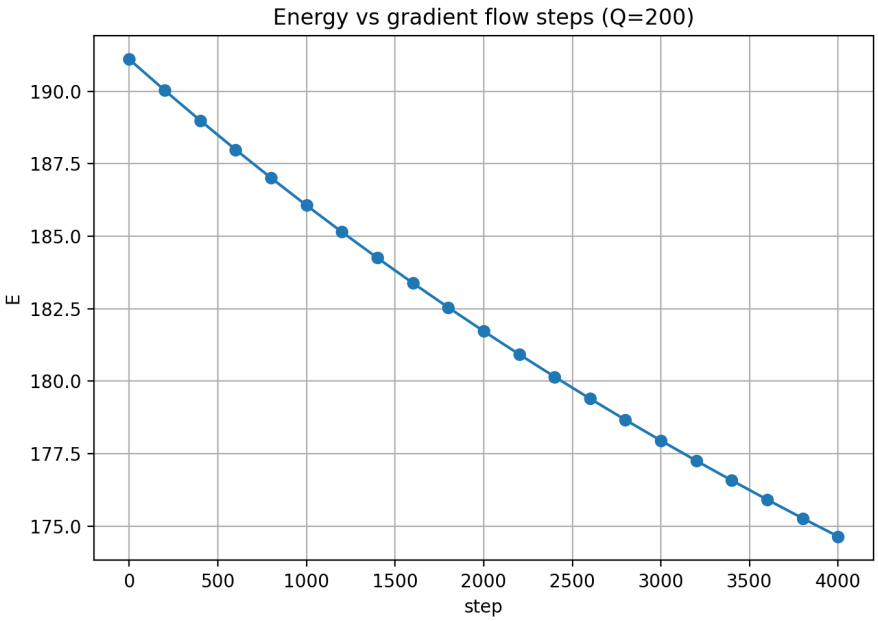

Figure 4: Energy density and internal phase flow for the toroidal configuration with $Q = 200$. The energy density is localized along the ring, while the phase gradient $\nabla\Theta_0$ shows the circulating motion around the major radius, which provides the effective centrifugal support for the torus.

7.6 Emergent geometry from motion

One of the conceptual motivations of this work is that geometry may emerge from organized motion rather than being an independent entity. The toroidal soliton provides a concrete example: the shape of the torus is not imposed externally but results from how the internal flows organize themselves.

The invariance of $(R_{\text{in}}, R_{\text{out}}, R_c, a)$ with respect to Q suggests that the geometry is fully determined by the structure of the internal flow, while the total energy simply scales with the amount of organized motion stored in the configuration.

8 Conclusion

We have shown that a simple nonlinear scalar field theory, interpreted as a continuum of organized motion, admits stable toroidal solitons that arise without external constraints or specialized potentials. These structures emerge from the interplay between internal rotation, nonlinear self-interaction, and quantized phase winding, which together produce self-consistent geometric confinement.

Using a combination of analytical arguments and high-resolution numerical simulations, we have constructed explicit stationary toroidal solutions and demonstrated their stability. The linear stability analysis, based on the second variation of the action, reveals that all nontrivial fluctuations possess positive frequency squared, with zero-modes corresponding only to global symmetries. This establishes the toroidal configuration as a genuine, dynamically stable soliton.

A key numerical result is that the toroidal geometry is essentially independent of the conserved charge Q: the inner radius, outer radius, core radius, and minor radius remain

fixed, while the energy-per-charge ratio E/Q decreases as Q increases. This supports a broader conceptual perspective: mass, energy localization, and geometric form may arise from organized patterns of motion rather than from separate fundamental entities.

In summary, the toroidal solitons presented here provide a new class of stable, self-organized configurations in scalar field theory, illustrating how geometry and mass can emerge from the dynamics of motion itself.

A Quadratic expansion and explicit form of the stability operator

In this appendix we provide the explicit quadratic expansion of the action around the stationary toroidal solution and derive the structure of the stability operator $\mathbf{K}$ appearing in the linear analysis.

A.1 Field decomposition in modulus and phase

Starting from the action

$$S = \int dt\, d^3x \left[|\partial_t \psi|^2 - |\nabla \psi|^2 - U(|\psi|) \right], \tag{14}$$

we write the complex field in polar form

$$\psi(t, \mathbf{x}) = \rho(t, \mathbf{x})\, e^{i\theta(t,\mathbf{x})}, \tag{15}$$

with $\rho \geq 0$ and $\theta \in \mathbb{R}$. In terms of (ρ, θ), the Lagrangian density becomes

$$\mathcal{L} = (\partial_t \rho)^2 + \rho^2 (\partial_t \theta)^2 - (\nabla \rho)^2 - \rho^2 (\nabla \theta)^2 - U(\rho). \tag{16}$$

The stationary toroidal background used in the main text is

$$\rho_0(\mathbf{x}) = \Phi_0(\mathbf{x}), \qquad \theta_0(t, \mathbf{x}) = \omega t + \Theta_0(\mathbf{x}), \tag{17}$$

where Φ_0 is time–independent and Θ_0 encodes the spatial winding (e.g. $\Theta_0 = n\varphi$ in adapted toroidal coordinates).

A.2 Perturbations around the toroidal background

We now perturb both modulus and phase,

$$\rho(t, \mathbf{x}) = \Phi_0(\mathbf{x}) + \delta\rho(t, \mathbf{x}), \qquad \theta(t, \mathbf{x}) = \omega t + \Theta_0(\mathbf{x}) + \delta\theta(t, \mathbf{x}), \tag{18}$$

with $\delta\rho$ and $\delta\theta$ small real perturbations. It is convenient to introduce the vector of fluctuations

$$\boldsymbol{\zeta} = \begin{pmatrix} \delta\rho \\ \delta\theta \end{pmatrix}. \tag{19}$$

In terms of these variables, the time derivatives entering Eq. (16) read

$$\partial_t \rho = \partial_t \delta\rho, \tag{20}$$

$$\partial_t \theta = \omega + \partial_t \delta\theta, \tag{21}$$

and the spatial gradients are

$$\nabla \rho = \nabla \Phi_0 + \nabla \delta\rho, \tag{22}$$

$$\nabla \theta = \nabla \Theta_0 + \nabla \delta\theta. \tag{23}$$

A.3 Expansion of the Lagrangian up to second order

We now expand $\mathcal{L}$ in powers of $(\delta\rho, \delta\theta)$ up to quadratic order. The background (Φ_0, Θ_0) is assumed to satisfy the stationary Euler–Lagrange equations, so all linear terms in the perturbations cancel after integration by parts, and the action can be written as

$$S = S[\Phi_0, \Theta_0] + S^{(2)}[\delta\rho, \delta\theta] + \mathcal{O}(\delta^3), \tag{24}$$

where $S^{(2)}$ collects all quadratic contributions.

From Eq. (16) we obtain the following pieces.

Time–derivative terms. Using

$$(\partial_t\rho)^2 = (\partial_t\delta\rho)^2, \tag{25}$$

and

$$\rho^2(\partial_t\theta)^2 = (\Phi_0 + \delta\rho)^2(\omega + \partial_t\delta\theta)^2, \tag{26}$$

we expand to quadratic order and, after subtracting background and linear terms, obtain

$$\mathcal{L}^{(2)}_{\text{time}} = (\partial_t\delta\rho)^2 + \Phi_0^2(\partial_t\delta\theta)^2 + 2\Phi_0\omega\,\delta\rho\,\partial_t\delta\theta + \omega^2(\delta\rho)^2. \tag{27}$$

Spatial–gradient terms. Similarly, the spatial part yields

$$\mathcal{L}^{(2)}_{\text{space}} = -(\nabla\delta\rho)^2 - \Phi_0^2(\nabla\delta\theta)^2 - 2\Phi_0\delta\rho\,\nabla\Theta_0\cdot\nabla\delta\theta - (\nabla\Theta_0)^2(\delta\rho)^2. \tag{28}$$

Potential term. Expanding the potential around Φ_0 gives

$$\mathcal{L}^{(2)}_{\text{pot}} = -\frac{1}{2}U''(\Phi_0)\,(\delta\rho)^2. \tag{29}$$

A.4 Quadratic action and stability operator

Collecting the contributions (27), (28) and (29), the full quadratic Lagrangian can be written as

$$\mathcal{L}^{(2)} = (\partial_t\delta\rho)^2+\Phi_0^2(\partial_t\delta\theta)^2+2\Phi_0\omega\,\delta\rho\,\partial_t\delta\theta-(\nabla\delta\rho)^2-\Phi_0^2(\nabla\delta\theta)^2-2\Phi_0\delta\rho\,\nabla\Theta_0\cdot\nabla\delta\theta-V_{\text{eff}}(\mathbf{x})\,(\delta\rho)^2, \tag{30}$$

where we have defined the effective potential

$$V_{\text{eff}}(\mathbf{x}) \equiv (\nabla\Theta_0)^2 + \frac{1}{2}U''(\Phi_0) - \omega^2. \tag{31}$$

This can be cast in matrix form as

$$\mathcal{L}^{(2)} = \frac{1}{2}\,\dot{\boldsymbol{\zeta}}^{\mathsf{T}}\mathbf{M}\dot{\boldsymbol{\zeta}} - \frac{1}{2}\,\boldsymbol{\zeta}^{\mathsf{T}}\mathbf{K}\boldsymbol{\zeta}, \tag{32}$$

with

$$\boldsymbol{\zeta} = \begin{pmatrix}\delta\rho\\ \delta\theta\end{pmatrix}, \qquad \dot{\boldsymbol{\zeta}} = \begin{pmatrix}\partial_t\delta\rho\\ \partial_t\delta\theta\end{pmatrix}, \tag{33}$$

and operator-valued matrices

$$\mathbf{M} = \begin{pmatrix}2 & 2\Phi_0\omega\\ 2\Phi_0\omega & 2\Phi_0^2\end{pmatrix}, \tag{34}$$

$$\mathbf{K} = \begin{pmatrix} -2\nabla^2 + 2V_{\rm eff}(\mathbf{x}) & 2\Phi_0\,\nabla\Theta_0\cdot\nabla \\ -2\nabla\cdot(\Phi_0\nabla\Theta_0\,\cdot) & -2\Phi_0^2\nabla^2 \end{pmatrix}. \tag{35}$$

The stability problem then reduces to the generalized eigenvalue equation

$$-\Omega^2\,\mathbf{M}\boldsymbol{\zeta} = \mathbf{K}\,\boldsymbol{\zeta}, \tag{36}$$

which, after a suitable change of variables to canonical kinetic terms, coincides with the eigenvalue problem used in the main text.

Strictly speaking, the mixed term $2\Phi_0\omega\,\delta\rho\,\partial_t\delta\theta$ introduces a gyroscopic structure rather than a purely symmetric kinetic matrix in the $(\delta\rho,\delta\theta)$ variables. In practice, the stability analysis is performed at the level of the normal–mode ansatz $e^{-i\Omega t}$ and by moving to a set of canonical fluctuation variables in which the kinetic form is diagonal. The explicit operator $\mathbf{K}$ used in the numerical diagonalization is therefore equivalent to the one obtained from the quadratic action, but written in a basis adapted to the normal modes.

References

[1] S. Coleman, *Q-balls*, Nucl. Phys. B **262**, 263–283 (1985).

[2] T. D. Lee and Y. Pang, *Nontopological solitons*, Phys. Rept. **221**, 251–350 (1992).

[3] R. Rajaraman, *Solitons and Instantons*, North–Holland, Amsterdam (1982).

[4] N. Manton and P. Sutcliffe, *Topological Solitons*, Cambridge University Press (2004).

[5] L. Pitaevskii and S. Stringari, *Bose–Einstein Condensation*, Oxford University Press (2003).

[6] R. Battye and P. Sutcliffe, *Knots as stable soliton solutions in a modified O(3) sigma model*, Phys. Rev. Lett. **81**, 4798 (1998).

[7] L. Faddeev and A. J. Niemi, *Stable knot-like structures in classical field theory*, Nature **387**, 58–61 (1997).

[8] E. Noether, *Invariante Variationsprobleme*, Nachr. d. König. Gesellsch. d. Wiss. zu Göttingen (1918). (English translation: Transp. Theory Stat. Phys. **1**, 186 (1971)).

[9] T. H. R. Skyrme, *A unified field theory of mesons and baryons*, Nucl. Phys. **31**, 556–569 (1962).

[10] T. Vachaspati, *Kinks and Domain Walls*, Cambridge University Press (2006).

[11] L. Pismen, *Vortices in Nonlinear Fields*, Clarendon Press, Oxford (1999).

[12] M. Gleiser, *Pseudostable bubbles*, Phys. Rev. D **49**, 2978 (1994).

[13] A. Kusenko, *Small Q balls*, Phys. Lett. B **404**, 285–290 (1997).

[14] P. Rosenau and J. M. Hyman, *Compactons: Solitons with compact support*, Phys. Rev. Lett. **70**, 564 (1993).

[15] P. W. Anderson, *Basic Notions of Condensed Matter Physics*, Addison–Wesley (1997).

[16] T. Dauxois and M. Peyrard, *Physics of Solitons*, Cambridge University Press (2006).

[17] D. Bazeia et al., *Compact structures in standard field theory*, Eur. Phys. J. C **79**, 1000 (2019).

[18] M. Hindmarsh and T. Kibble, *Cosmic strings*, Rept. Prog. Phys. **58**, 477 (1995).

[19] G. E. Volovik, *The Universe in a Helium Droplet*, Oxford University Press (2003).